CHIN. PHYS. LETT. Vol. 36, No. 1 (2019) 017801

A Novel Method for PIT Effects Based on Plasmonic Decoupling *

Bin Sun(孙斌)[1**], Fei-Feng Xie(谢飞凤)[1], Shuai Kang(康帅)[1],
You-chang Yang(杨友昌)[1], Jian-Qiang Liu(刘坚强)[2]

[1]*Department of Physics, Zunyi Normal College, Zunyi 563002*
[2]*College of Science, Jiujiang University, Jiujiang 332005*

(Received 3 September 2018)

A tunable dual-band stop-band THz spectrum can be realized in a hybrid structure, which consists of metal nanoribbon arrays clad by graphene nanoribbons. Dual-band spectra can be controlled separately by the nanoribbon width w and graphene chemical potential μ_c. We explain that two local plasmonic modes excited at graphene ribbons belong to different gratings, which uncouple with each other by electro-magnetic shielding of the metal ribbons. Furthermore, plasmonic induced transparent (PIT) effects can also be realized by making the two transmission notches close to each other, with better performance than the PIT system based on plasmonic coupling, such as with a larger extinction radio and a tunable transparency window.

PACS: 78.67.Wj, 78.20.−e, 78.67.Pt, 78.66.−w DOI: 10.1088/0256-307X/36/1/017801

Terahertz surface plasmon polaritons (SPPs) are sub-wavelength charge density oscillations coupling with terahertz electromagnetic fields.[1−3] Recently SPPs with tightly confined volume and less propagating loss have been found on a doped graphene incident by terahertz light, which have been experimentally demonstrated[4,5] and are named graphene surface plasmon polaritons (GSPPs).[6] When graphene structures are finite-sized, graphene localized surface plasmon (GLSP) characterized by alternating charge accumulation at the opposing edges of the graphene is excited, which allows a strong interaction between THz light and materials. The excitation of SPPs occurs only in a narrow spectral band, which is determined by specific type of metal and geometrical details of the nanostructures. Multi-band response[7] could be realized in hybrid nanostructures due to the strong plasmonic coupling between plasmonic modes, such as a kind of splitting SPP modes,[8] are designed for mode interference between bright antibonding dipole mode of split disks and subradiant mode supported by the narrow split gap. Hybrid nanostructures are composited of a single material[9−13] or multi-kind of materials,[14,15] resulting in support for hybrid modes.[9,10,16] Recently, hybrid structures that consist of graphene and metal have attracted considerable attention because of their potential application. Gu *et al.* found extremely confined THz SPPs in graphene-metal structures.[17] A tunable THz technology based on hybrid metal-graphene plasmons[18] has been experimentally demonstrated. Thongrattanasiri *et al.* have designed periodically patterned graphene on a dielectric film on top of a thick metal for complete THz optical absorption.[19] Although both graphene and metal can be used as THz metamaterials, the size of the devices made from them are different: metal is μm-sized, while it is nano-sized for graphene. This indicates that graphene-based metamaterials are more compatible in size with electronic device than metal. Furthermore, metallic structures are easily manufactured, shaped and behave as perfect electric conductor (PEC) in THz. Thus, the advantages of graphene and metal could be combined to improve the performance of optical nano-devices.

Recently, the low coupling efficiency of GLSP between plasmonic modes and narrow bandwidth of GLSP greatly limits its applications in nanophotonic functionalities.[20] However, in most of the reported PIT effects,[21,22] there are several shortcomings; for instance, PIT resonant wavelength is fixed after the structure is designed, the width of PIT window is untunable or extinction radio (ER) is not enough for practical applications. Because most of the reported PIT effects are based on plasmonic coupling between a bright mode and a dark mode, this results in its sensitivity to their coupling strength. In other words, PIT effects would get worse or even disappear when the coupling between two plasmonic modes is weak. Consequently, the structure parameters for strong coupling need to be carefully designed. To overcome these shortcomings, PIT based on new materials or novel methods is urgent required for practical applications.

In this work, we design a simple hybrid structure consisting of metal nanoribbons array cladding by graphene nanoribbons, which exploits both the advantages of graphene and metal. By exciting two un-

*Supported by the Key Disciplines of Physics of Guizhou Province under Grant No QXWB[2013]18, the Major Research Projects for Innovation Groups of Guizhou Province under Grant No KY[2018]028, the National Natural Science Foundation of China under Grant No 11464052, the Science and Technology Foundation of Guizhou Province under Grant No J[2015]2149, the Youth Foundation of the Education Department of Guizhou Province under Grant No KY[2017]248, the Startup Foundation for Doctors of Zunyi Normal University under Grant No 40300326, and the Natural Science Foundation of Jiangxi Province under Grant No 20161BAB201002.

**Corresponding author. Email: sunbin@hnu.edu.cn

© 2019 Chinese Physical Society and IOP Publishing Ltd

coupled GLSPs at graphene nanoribbons due to metal isolation, a dual-band is filtered in the transmission spectrum. Furthermore, the GLSP wavelength can be independently tunable due to the tunable surface conductivity of the graphene. Moreover, PIT can also be realized by moving two GLSP resonant wavelengths as close as possible, which is a novel method for realizing tunable THz PIT effects in nanoscale. Furthermore, we achieve larger ER of 77.8% than that reported.[22] The proposed structure derived in our work seems to be very promising for new THz absorbers in hybrid metasurface or realizing phototonic devices based on plasmonic decoupling.

A metallic nanoribbon grating is symmetrically sandwiched by two graphene nanoribbon gratings that are infinitely long in the z direction, as shown in Fig. 1, forming a hybrid graphene/metal multilayered subwavelength metasurface.[23–25] A space gap of g is set between graphene and metal nanoribbons to prevent potential carrier injections from the graphene layer into the metal.[26] The three stacked gratings are set to the same period of p. The width of the top doped graphene ribbons, central metal ribbons and the bottom ones are w_1, w_m and w_2, respectively. For simplicity, we set $w_\mathrm{m} = \max(w_1, w_2)$. We calculate the transmission through the composite system by a 2D finite element method (FEM) using commercial software (Comsol Multiphysics). First, the whole structure is embedded in air. The x-polarized (the electric field is perpendicular to the graphene nanoribbons) light with a wavelength λ is normally incident from the top of the structure. The metal, typically gold or silver, is modeled as a PEC, which is a good approximation here for the THz frequency range. We use the Kubo formula,[19,27,28] for the complex surface conductivity of graphene, which is a function of the angular frequency ω (wavelength λ), chemical potential μ_c (also Fermi level E_F), temperature T and the electron-phonon scattering rate γ (inverse of momentum relaxation time τ, $\gamma = \tau^{-1} = eV_\mathrm{F}^2/(n\mu_\mathrm{c})$, where n, V_F and $-e$ are graphene carries mobility, the femivelocity and the charge of an electron, respectively). Within the random-phase approximation, the surface graphene conductivity $\sigma(\omega, \mu_\mathrm{c}T, \gamma)$ can be simplified to a complex formulation consisting of interband and intraband contributions in the absence of an external magnetic field. The intraband term can be evaluated as

$$\sigma_\mathrm{intra}(\omega, \mu_\mathrm{c}, T, \tau) = -\frac{je^2 k_\mathrm{B} T}{\pi\hbar^2(\omega - j\gamma)}\left[\frac{\mu_\mathrm{c}}{k_\mathrm{B}T} + 2\ln(e^{\frac{\mu_\mathrm{c}}{k_\mathrm{B}T}} + 1)\right], \quad (1)$$

and the interband term is approximated, for $k_\mathrm{B}T \ll |\mu_\mathrm{c}|$, $\hbar\omega$ by

$$\sigma_\mathrm{inter}(\omega, \mu_\mathrm{c}, T, \tau) = -\frac{je^2}{4\pi\hbar}\ln\left[\frac{2|\mu_\mathrm{c}| - (\omega - j\gamma)}{2|\mu_\mathrm{c}| + (\omega - j\gamma)}\right], \quad (2)$$

where $\hbar$ is the reduced Planck's constant. From Eqs. (1) and (2), it is found that in the THz and far-infrared regions, the intraband contribution dominates, while interband contribution becomes pronounced in the near-infrared and visible regions. Moreover, the fact that the parameter of temperature T only exists in the intraband term indicates that GLSP is greatly sensitive to the temperature, such that a ambient temperature $T = 300\,\mathrm{K}$ is chosen for representing a room temperature. In the considered model, the double graphene nanoribbons could be doped as μ_c1 and μ_c2 by a split gate device applying different bias voltages of V_1 and V_2, respectively, as shown in Fig. 1.

Graphene is a one-atom-thick material with a thickness of 0.34 nm, which is the thinnest material existing in nature. In implementation, to save computing time and storage space, we define the graphene as having a thickness of $\Delta = 1\,\mathrm{nm}$. We should point out that this is enough to validate our numerical simulations although other extremely small values for this thickness lead to similar results. Therefore, the corresponding volume conductivity of the bulk material is σ/Δ. The equivalent permittivity of the Δ-thick graphene layer is given by $\epsilon_\mathrm{g,eq} = 1 + i\sigma\eta_0/(k_0\Delta)$, where $\eta_0(\approx 377\Omega)$ is the impedance of air, and $k_0 = 2\pi/\lambda$. Adaptive triangle meshing with a minimum feature resolution of 0.2 nm has been used in the simulations. Periodic boundary conditions are set in the x direction and perfectly matched layer (PML) for the truncation of open boundaries in the y direction.

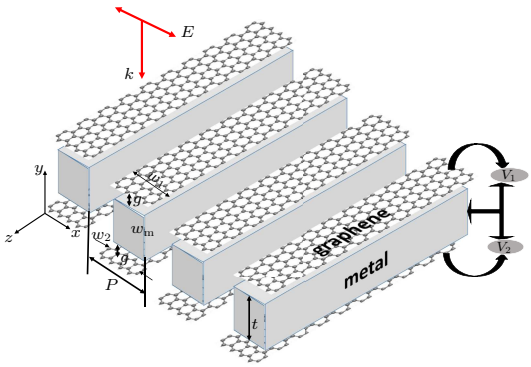

Fig. 1. Schematic diagram of a unit of the graphene/metal hybrid structure. The structure is illuminated by a normally incident plane wave polarized in the x direction.

When a graphene film is patterned to nanometer dimensions, the restricted free carriers oscillate with the electric field of EM waves, resulting in a GLSP. The GLSP in isolated graphene-metal ribbons can be governed by a quasi-static theory. If the damping is not large, then the resonant frequency ω_0 can be approximately calculated by

$$\omega_0 = A\sqrt{(e^2\mu_\mathrm{c})/(\hbar^2\epsilon_\mathrm{eff}w)}, \quad (3)$$

where A is a scale coefficient, w is the ribbon width, and ϵ_eff is the effective dielectric constant of the surrounding medium. It is found that the resonant GLSP

frequency linearly scales with $\sqrt{\mu_c/w}$. Thus, it is easy to conclude that the plasmonic mode excited in the model is a GLSP because the response of the proposed hybrid structure possesses the same behavior.

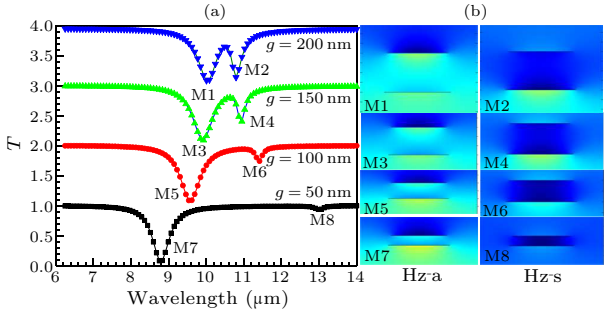

Fig. 2. (a) Transmission of double graphene grating with nanogap of $g = 50$, 100, 150 and 200 nm, of which transmission spectra are Y offset one by one for clearly showing the coupling effects. (b) Hz field for modes at the minimal transmission, respectively. The Hz-a (Hz-s) represent antisymmetrical (symmetrical) coupling of GLSP.

Figure 2 (a) present transmission spectra of double uncontacted graphene nanoribbons array stacked vertically with gaps of $g = 50$, 100, 150 and 200 nm, while other structure parameters of $p = 400$, $w_1 = 190$, $w_2 = 210$ nm and $\mu_{c1} = \mu_{c2} = 0.5$ eV are held constant. The doped graphene nanoribbon grating with different widths should support two GLSP modes whose resonant wavelengths are dependent on their ribbon widths without respect to the plasmonic coupling between the nearby ribbons. From Fig. 2(a), it can be noted that two pronounced transmission dips correspond two GLSP modes at different wavelengths but they gradually increase separation as the gap width reduces. Meanwhile, the GLSP corresponding to the longer resonant wavelength becomes weak and disappears almost finally. It could be attributed to the strong plasmonic coupling between the GLSP modes excited in the two graphene nanoribbons. We also plot the contour profiles of field Hz of modes corresponding to the dips in spectra as shown in Fig. 2(b). Note that the modes denoted as M1, M3, M5 and M7 (M2, M4, M6 and M8) originate from the antisymmetric (symmetric) coupling of GLSP. Consequently, the strong coupling between GLSP modes makes the dual-band response unstable and uncontrollable. Naturally, one would wonder how to make double graphene gratings with an obvious dual-band response while as far as possible keeping the smaller thickness of the multilayers.

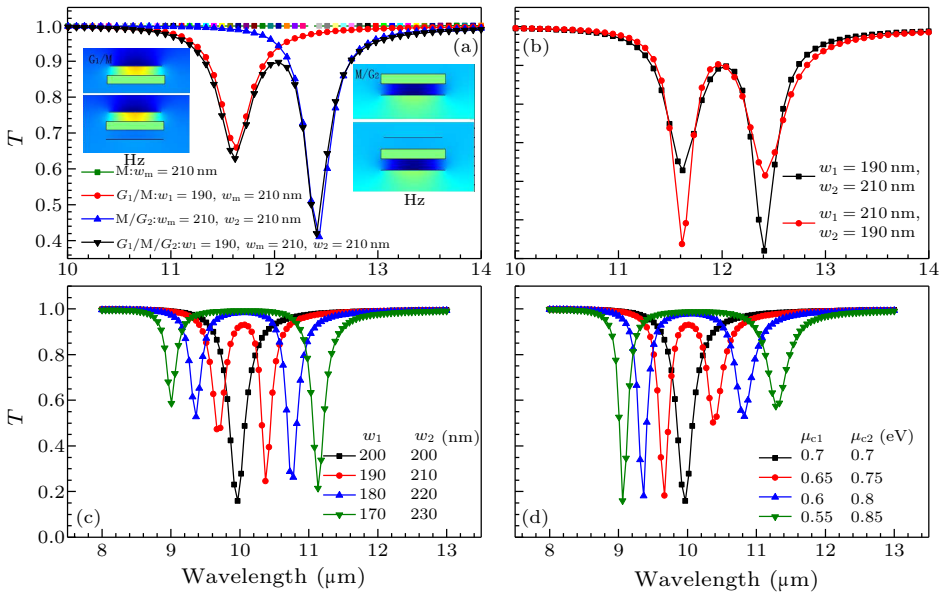

Fig. 3. (a) Transmission spectra of $G_1/M/G_2$, G_1/M and G_2/M structures with $p = 400$ nm and $\mu_{c1} = \mu_{c2} = 0.5$ eV. Insets: the Hz field distribution of the corresponding GLSP. (b) Transmissions of $G_1/M/G_2$ and $G_2/M/G_1$ systems (in the reverse situation). Dual-band spectra for (c) different nanoribbon widths and (d) different chemical potentials.

Metal nanoribbons are inserted in space between graphene nanoribbons, thus forming a graphene-metal-graphene ($G_1/M/G_2$) grating. To miniaturize the device, the graphene/metal gap g, the grating period p and the metal thickness t are fixed as $g = 35$ nm, $p = 400$ nm and $t = 30$ nm, respectively, in the simulation unless otherwise stated. In Fig. 3(a), transmission spectra are calculated for $G_1/M/G_2$ with graphene chemical potential $\mu_{c1} = \mu_{c2} = 0.5$ eV, $w_1 = 190$ nm and $w_2 = 210$ nm, respectively. Note that an obvious dual-band centered at incident wavelengths $\lambda = 11.6$ and 12.5 μm is observed, which is very different from the situation in the structure of two graphenes grating without a metal grating. For a deeper insight into how the dual-band stopband spectra are formed, the structures of graphene-metal (G_1/M) grating and metal-graphene (M/G_2) grating with the same parameters as in the $G_1/M/G_2$ system are also simulated. Compared with transmissions of G_1/M and M/G_2, the resonant frequencies indicated by the dips in the transmission

spectra coincide with the dips for the $G_1/M/G_2$ system. In other words, the $G_1/M/G_2$ system has the same resonant wavelength as the G_1/M and M/G_2 systems. This can explain why the GLSPs excited in two nearby located graphene nanoribbons decouple with each other. The contour profiles of the field Hz at transmission peaks for those three structures are also shown in insets of Fig. 3(a), respectively. Note that metal-confined GLSP modes are exited in the graphene ribbon where the EM field is isolated by the metal ribbon. Thus, it is not difficult to understand that the field distribution of GLSP mode in $G_1/M/G_2$ is almost the same as those in G_1/M and M/G_2.

In Fig. 3(b), the transmission spectra of $G_1/M/G_2$ and $G_2/M/G_1$ with $w_1 = 190$, $w_2 = 210$ nm are calculated, respectively, for comparison. Clearly, one can find that asymmetry appears in dual-band spectra. Furthermore, the GLSP modes excited in graphene ribbons located at the output side show the deeper dips in transmission spectra of such two cases. This can be explained as follows: because the double-layer graphene ribbons sandwiching the metal ribbons act as two uncoupled resonator(antenna), the up and down resonator directly supports the GLSP mode at different wavelengths, resulting in location-dependent GLSP mode. Because the metal nanoribbons behave as electromagnetic radiation antenna, the GLSP modes above/below the metal ribbon radiate in the $-y/+y$ direction, resulting in larger/smaller EM energy for transmission. So, the asymmetric transmission spectra can be mainly attributed to the asymmetric radiation of GLSP modes.

Based on these discussions, one could precisely control two different GLSP modes in the nano-sized system without respect to the mode coupling between them. In other words, we can freely tune the locations of two dips in transmission spectra by changing the width of nanoribbon or the graphene doping level. In Fig. 3(c), the dual-band moves linearly close to each other as the difference of the two ribbon widths decreases, until they finally overlap. We also obtain the same effects through the chemical potential by gate voltage, as shown in Fig. 3(d). In general, one could move two dips as close as possible, resulting a narrow transparency window (namely, a PIT effects) formed. Moreover, the extinction radio (ER) for PIT is defined by ER=$(1-T_{\min}/T_{\max})\%$, representing modulation efficiencies in transmission. One notes that PIT effects obviously emerge when $w_1 = 190$, $w_2 = 210$ nm in Fig. 3(c) and $u_{c1} = 0.65$, $u_{c2} = 0.75$ eV in Fig. 3(d), where a narrow window with $T_{\max} = 0.9$, $T_{\min} = 0.2$, thus ER can reach 77.8%.

Figures 4(a) and 4(b) show PIT spectra as a function of the nanoribbons' width and chemical potential, respectively. A small difference of 20 nm between the two graphene nanoribbons width with the same doping level of 0.5 eV induces a narrow window of < 1 μm width band. The location of PIT window is linearly changed with the nanoribbon width, as shown in Fig. 4(a). The bandwidth of the PIT window depends on the width difference between the top and down graphene nanoribbons. In addition, metal ribbons forming an even ground plane act as a patterned gate for ribbon-like doping area in graphene. By adding a electrical gate at graphene and metal nanoribbons with different voltages, a difference of 0.1 eV in chemical potential between up and down graphene ribbons could be realized, resulting in electrical tunable PIT effects, as shown in Fig. 4(b). One also notes that the locations of PIT window in transmission spectra are blue shifted as the whole doping level of the graphene increases. Meanwhile, the band width of the transparent window becomes narrower.

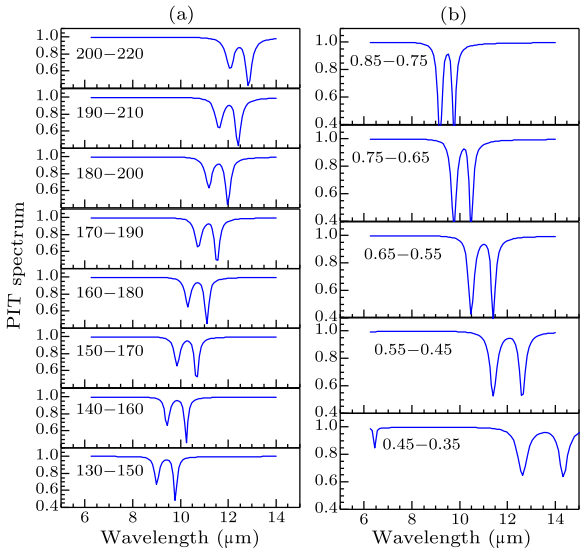

Fig. 4. PIT spectra of $G_1/M/G_2$ system with (a) different graphene nanoribbon widths w (nm) and (b) with different chemical potentials $u_{c1} \neq u_{c2}$ (eV).

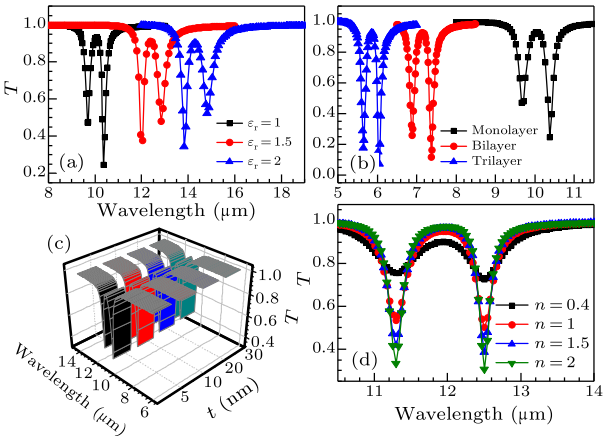

Fig. 5. PIT spectra of $G_1/M/G_2$ versus (a) environment relative permittivity ϵ_r, (b) graphene layer numbers N, (c) metal thickness t and (d) carrier mobilities n.

For practical situations, a dielectric should be considered in which the hybrid model is embedded. Thus transmission spectra for various dielectrics with permittivities of 1 (air), 1.5 (liquid CO_2) and 2(SiO_2)

are simulated, respectively, as shown in Fig. 5(a). Obviously, PIT effects also keep working for graphene nanoribbons with $w_1 = 190\,\text{nm}$ and $w_2 = 210\,\text{nm}$ with the same doping level of $u_{c1} = u_{c2} = 0.7\,\text{eV}$ with different dielectrics. Moreover, PIT windows in spectra are red-shifted as the environment dielectric index increases. The number of graphene layers is another important factor for controlling THz waves due to the fact that the surface conductivity of a few layers of graphene is $N\sigma_g$, where N is the number of graphene layers and is smaller than six. The PIT spectra of the hybrid model embedded in air with the same structure parameters are shown in Fig. 5(a), which are calculated for different layer numbers N ($N = 1$, 2 and 3 corresponding to monolayer, bilayer and tri-layer, respectively), as shown in Fig. 5(b). Note that the PIT window is blue-shifted and becomes narrower as the layer number increases.

In the structure, the thickness of metal is important because it determines the distance between graphene ribbons. In general, if the distance is small, then the coupling of the plasmonic modes cannot be ignored. We also calculate the influence of metal thickness on the PIT effects. PIT spectra of $G_1/M/G_2$ with $\mu_{c1} = 0.55\,\text{eV}$ and $\mu_{c2} = 0.65\,\text{eV}$ and $w_1 = w_2 = 200\,\text{nm}$ for different metal thicknesses are shown in Fig. 5(c). Surprisingly, the PIT spectra are almost unchanged with the metal thickness t, changing in the range of 5–30 nm.

Based on this analysis, it can be seen that the ER of the notch in the transmission spectra is not large enough for applications. In general, the GLSP notches in the transmission spectra are determined by the optical loss in graphene, which are mainly characterized by the real part of the conductivity at the operating mid-IR frequency. Thus, we could control the ER by changing the real part of the conductivity, which linearly relies on the carrier mobility of graphene. However, the CVD graphene generally has a mobility below $1\,\text{m}^2/(\text{V}\cdot\text{s})$ due to the point defects and residue impurities introduced during growth or transfer of graphene. The electron mobility in an exfoliated graphene can exceed $2.3\ \text{m}^2/(\text{V}\cdot\text{s})$.[29] The PIT spectra of $G_1/M/G_2$ with $\mu_{c1} = 0.55\,\text{eV}$, $\mu_{c2} = 0.45\,\text{eV}$ and $w_1 = w_2 = 200\,\text{nm}$ for different carriers mobilities are shown in Fig. 5(d). Note that the notches in PIT spectra become broader and shallower as n reduces from $2\,\text{m}^2/(\text{V}\cdot\text{s})$ to $0.4\,\text{m}^2/(\text{V}\cdot\text{s})$ due to the lower mobility, which corresponds to higher loss. When the mobility increases to $n = 2\,\text{m}^2/(\text{V}\cdot\text{s})$, the ER reaches 70%, which is larger than 16.7% at $n = 0.4\,\text{m}^2/(\text{V}\cdot\text{s})$.

In summary, we have realized a tunable dual-band THz filter by two graphene nanoribbons isolated by metal nanoribbons. By exciting two uncoupled GLSPs in graphene nanoribbons due to metal isolation, a dual-band transmission spectrum can be filtered. Furthermore, the stop bands can be independently controlled by the geometrical parameters of the graphene nanoribbons, including the nanoribbons' width and gate voltage, and so on. Moreover, PIT can also be realized by moving the GLSP resonant wavelength as close as possible, which is a novel method for realizing tunable THz PIT effects in the nanoscale. Furthermore, we achieve a deeper ER at 77.8% better than that reported.[22] The rich results derived in our work will give a theoretical guide for a new THz absorber in hybrid metamaterial and to realize phototonic devices based on plasmonic decoupling.

References

[1] Vakil A and Engheta N 2011 *Science* **332** 1291
[2] Liu H, Ren G, Gao Y, Zhu B and Wu B 2016 *Plasmonics* **11** 411
[3] Wang P D, Jia Z Y and Cheng N P 2018 *Chin. Phys. B* **27** 57101
[4] Fei Z, Rodin A S, Andreev G O, Bao W, McLeod A S, Wagner M, Zhang L M, Zhao Z, Thiemens M and Basov D N 2012 *Nature* **487** 82
[5] Chen J et al 2012 *Nature* **487** 77
[6] Lin I T, Fan C and Liu J M 2017 *IEEE J. Sel. Top. Quantum Electron.* **23** 1
[7] Li H P, Fu W Y, Shen X P, Hua K and Wang W H 2017 *Chin. Phys. B* **26** 127801
[8] Zhang S, Li G C, Chen Y, Zhu X, Liu S D, Lei D Y and Duan H 2016 *ACS Nano* **10** 11105
[9] Christensen J, Manjavacas A, Thongrattanasiri S, Koppens F H L and García de Abajo F J 2011 *ACS Nano* **6** 431
[10] Sun Y, Zheng Z, Cheng J, Liu J, Liu J and Li S 2013 *Appl. Phys. Lett.* **103** 6
[11] He S, Yang M and Wang R Q 2018 *Chin. Phys. B* **27** 47303
[12] Zhang Q and Zhang H 2018 *Chin. Phys. B* **27** 27301
[13] Fan Y, Chen C and Li D G 2017 *Chin. Phys. B* **26** 17302
[14] Tan S, Argondizzo A, Ren J, Liu L, Zhao J and Petek H 2017 *Nat. Photon.* **11** 806
[15] Bafandeh N, Larijani M M, Shafiekhani A, Hantehzadeh M R and Sheikh N 2016 *Chin. Phys. Lett.* **33** 117801
[16] Chen J, Mao P, Xu R, Tang C, Liu Y, Wang Q and Zhang L 2015 *Opt. Express* **23** 16238
[17] Gu X F, Lin I T and Liu J M 2013 *Appl. Phys. Lett.* **103** 071103
[18] Jadidi M M, Sushkov A B, Myers-ward R L, Boyd A K, Daniels K M and Gaskill D K 2015 arXiv:1506.05817v2
[19] Thongrattanasiri S, Koppens F H L and García de A F J 2012 *Phys. Rev. Lett.* **108** 047401
[20] Zuo R, Liu W, Cheng H, Chen S and Tian J 2018 *Adv. Opt. Mater.* **6** 1800795
[21] Duan X, Chen S, Cheng H, Li Z and Tian J 2013 *Opt. Lett.* **38** 483
[22] Cheng H et al 2013 *Appl. Phys. Lett.* **103** 203112
[23] Liu W, Li Z, Cheng H, Tang C, Li J, Zhang S, Chen S and Tian J 2018 *Adv. Mater.* **30** 1706368
[24] Liu H, Zhu J P, Wang K, Wang X H and Xu R 2016 *Chin. Phys. Lett.* **33** 064204
[25] Han W et al 2016 *Chin. Phys. Lett.* **33** 027803
[26] Li F and Wu H 2016 *Chin. Phys. Lett.* **33** 067101
[27] Chen P Y and Alù A 2011 *ACS Nano* **5** 5855
[28] Gusynin V P, Sharapov S G and Carbotte J P 2007 *J. Phys.: Condens. Matter* **19** 026222
[29] Bolotin K I, Sikes K J, Jiang Z, Klima M, Fudenberg G, Hone J, Kim P and Stormer H L 2008 *Solid State Commun.* **146** 351